



Coherent Control of a Single ^{29}Si Nuclear Spin Qubit

Jarryd J. Pla,^{1,2,*} Fahd A. Mohiyaddin,^{1,2} Kuan Y. Tan,^{1,2} Juan P. Dehollain,^{1,2} Rajib Rahman,³ Gerhard Klimeck,³ David N. Jamieson,^{4,5} Andrew S. Dzurak,^{1,2} and Andrea Morello^{1,2,†}

¹Centre of Excellence for Quantum Computation and Communication Technology, Sydney, New South Wales 2052, Australia

²School of Electrical Engineering and Telecommunications, The University of New South Wales Australia, Sydney, New South Wales 2052, Australia

³Network for Computational Nanotechnology, Purdue University, West Lafayette, Indiana 47907, USA

⁴Centre of Excellence for Quantum Computation and Communication Technology, Melbourne, Victoria 3010, Australia

⁵School of Physics, University of Melbourne, Melbourne, Victoria 3010, Australia

(Received 14 July 2014; revised manuscript received 11 November 2014; published 9 December 2014)

Magnetic fluctuations caused by the nuclear spins of a host crystal are often the leading source of decoherence for many types of solid-state spin qubit. In group-IV semiconductor materials, the spin-bearing nuclei are sufficiently rare that it is possible to identify and control individual host nuclear spins. This Letter presents the first experimental detection and manipulation of a single ^{29}Si nuclear spin. The quantum nondemolition single-shot readout of the spin is demonstrated, and a Hahn echo measurement reveals a coherence time of $T_2 = 6.3(7)$ ms—in excellent agreement with bulk experiments. Atomistic modeling combined with extracted experimental parameters provides possible lattice sites for the ^{29}Si atom under investigation. These results demonstrate that single ^{29}Si nuclear spins could serve as a valuable resource in a silicon spin-based quantum computer.

DOI: 10.1103/PhysRevLett.113.246801

PACS numbers: 73.22.-f, 73.23.-b, 76.30.-v, 76.60.-k

The presence of nonzero nuclear spins in a host crystal lattice is known to induce decoherence in a central spin qubit through mechanisms such as spectral diffusion [1]. This “nuclear bath” is the primary source of decoherence for ^{31}P electron and nuclear spin qubits in silicon [2,3], nitrogen-vacancy (NV) centers in diamond [4], as well as for GaAs-based quantum dot spin qubits [5,6]. However, for semiconductors composed of a majority of spin-zero isotopes (such as silicon and carbon), the low abundance of spin-carrying nuclei allows us to resolve the hyperfine couplings of individual nuclei with a central electronic spin, permitting the detection and manipulation of single nuclear spins. This has led to the demonstration of a quantum register for the spin of a NV center in diamond, where the electronic spin state can be stored in individual nuclei [7] and read out in a single shot [8]. Quantum error correction protocols have been implemented within these nuclear spin registers [9,10], showing their potential to implement surface-code based quantum computing architectures [11]. Natural silicon contains a 4.7% abundance of the spin-carrying ($I = 1/2$) ^{29}Si isotope which, in combination with a localized electron spin, could, in principle, be used as a quantum register or ancilla qubit equivalent to ^{13}C in NV diamond. In addition, the ^{29}Si nuclear spin has itself been championed as a quantum bit in an “all-silicon” quantum computer [12,13].

Here, we present the first experimental demonstration of single-shot readout, coherent control, and measurement of the coherence properties of an individual ^{29}Si nuclear spin in natural Si coupled to a ^{31}P donor. The ^{31}P donor in

silicon consists of an electron spin ($S = 1/2$) bound at cryogenic temperatures to the ^{31}P nucleus, with spin $I = 1/2$. The eigenstates of this system are displayed as an inset to Fig. 1(a), with thin arrows representing the spin state of the electron (\uparrow, \downarrow) and thick arrows representing the ^{31}P nucleus ($\uparrow_{\text{P}}, \downarrow_{\text{P}}$). In the absence of coupling to other spins, the ^{31}P donor exhibits two electron spin resonance (ESR) frequencies $\nu_{e1,2}$, and two ^{31}P nuclear magnetic resonance (NMR) frequencies $\nu_{n1,2}$. The presence of ^{29}Si nuclear spins (with states written as $\uparrow_{\text{Si}}, \downarrow_{\text{Si}}$) introduces additional features, which are the focus of this work.

The experiments presented here follow from previous work where the electron [2] and nuclear [3] spins of a single ^{31}P donor were addressed using a compact nanoscale device [14] consisting of ion-implanted phosphorus donors [15], tunnel coupled to a silicon MOS single-electron transistor (SET) [16]. All measurements were performed with a magnetic field $B_0 = 1.77$ T, in a dilution refrigerator with electron temperature $T_{\text{el}} \approx 250$ mK. Under these conditions, spin-dependent tunneling occurs between the donor and the SET island when their electrochemical potentials are aligned. A donor \rightarrow SET tunneling event constitutes the single-shot readout of a $|\uparrow\rangle$ electron and is followed by a preferential $|\downarrow\rangle$ initialization [17]. Spin control was achieved through microwave and rf excitations generated by an on-chip broadband transmission line [18]. The device and experimental setup employed here are identical to those used in our previous work [2,3].

The detection of a single ^{29}Si spin was achieved by first performing an ESR experiment for a fixed orientation of the

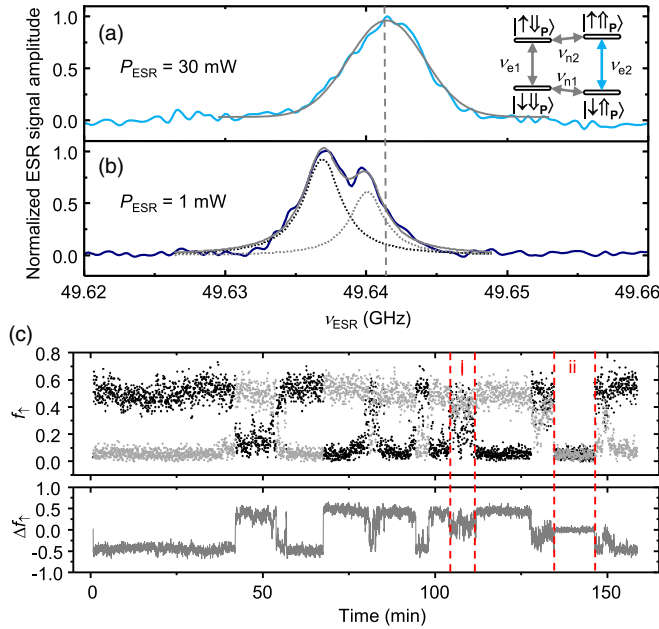


FIG. 1 (color online). ESR scans at the electron spin transition corresponding to the ^{31}P nuclear $|\uparrow_{\text{P}}\rangle$ state (ν_{e2}), performed using microwave powers of (a) $P_{\text{ESR}} = 30$ mW and (b) $P_{\text{ESR}} = 1$ mW. The data in (a) is fit with a Gaussian line shape (gray line). The low-power peak in (b) displays a splitting of ~ 2.2 MHz and is fit with a double-Lorentzian curve (gray line is the sum of the dotted lines). Inset of (a): energy level diagram of the ^{31}P donor system. The ^{29}Si experiments are performed around the ν_{e2} resonance. (c) Single-shot readout of a ^{29}Si nuclear spin. Quantum jumps of the nuclear spin occur on minute-long time scales, with no clear preference for the orientation. Bottom panel: difference in the spin-up fraction Δf_{\uparrow} from measurements on the left and right sides of the split ν_{e2} resonance (shown individually in the top panel). Region (i) highlights an instance where the remaining ^{29}Si nuclear spin bath is configured in such a way that resonance is in between the two peaks of panel (b), and the ^{29}Si nuclear spin state is, therefore, unresolvable. In region (ii), the ^{31}P nuclear spin has flipped to the $|\downarrow_{\text{P}}\rangle$ state.

^{31}P nuclear spin. We chose the transition corresponding to the $|\uparrow_{\text{P}}\rangle$ state, i.e., ν_{e2} , since the nuclear spin is predominantly polarized here as a result of the differing $|\uparrow_{\text{P}}\rangle$ and $|\downarrow_{\text{P}}\rangle$ nuclear spin relaxation mechanisms [3]. The ESR experiment involves using the SET to monitor the induced electron spin-up fraction f_{\uparrow} in response to a microwave excitation with varying frequency ν_{ESR} , resulting in the spectrum of Fig. 1(a). The line shape is well described by a Gaussian with full width at half maximum (FWHM) ~ 7 MHz (or $250 \mu\text{T}$) at the largest applied ESR power $P_{\text{ESR}} \approx 30$ mW. This figure corresponds to the bulk value for the inhomogeneous broadening caused by the ^{29}Si nuclear spin bath [19]. From the measured Rabi frequency at this power [2], we extract $B_1 \approx 120 \mu\text{T}$, confirming that power broadening does not occur here. However, by further reducing the excitation power to 1 mW ($B_1 \approx 22 \mu\text{T}$), the ESR line splits in two and shifts to a lower frequency [Fig. 1(b)]. A double-Lorentzian fit best captures the shape

of the line and yields a FWHM ≈ 3 MHz for both peaks, with the center frequency decreasing by 3 MHz with respect to Fig. 1(a). Overall, the observed low-power behavior indicates a polarization and a narrowing of the ^{29}Si nuclear bath. The behavior is reproducible over several measurements and does not depend on the direction of the frequency sweep. The microscopic origin of this phenomenon is consistent with the standard Overhauser effect, where excitation of the electron spin to the $|\uparrow\rangle$ state, in combination with a fast electron-nuclear spin-conserving relaxation channel $|\uparrow\downarrow_{\text{Si}}\rangle \rightarrow |\downarrow\uparrow_{\text{Si}}\rangle$, results in a predominant $|\uparrow_{\text{Si}}\rangle$ bath polarization [20]. The line shift to lower frequencies is a result of the negative gyromagnetic ratio of ^{29}Si , $\gamma_{\text{Si}} = -8.458$ MHz/T (see Ref. [21]).

The splitting of the ν_{e2} line indicates the presence of a single ^{29}Si nuclear spin, strongly hyperfine-coupled to the donor-bound electron. This allows us to read the ^{29}Si spin state in the same way as the ^{31}P nuclear spin [3]. Here, we apply adiabatic frequency sweeps [22] over the left half of the ν_{e2} resonance, i.e., from far detuned to a point midway between the two peaks. After each passage, we acquire a single-shot measurement of the electron spin to obtain f_{\uparrow} . The process is then repeated on the right half of the hyperfine-split ν_{e2} peak. We observe clear “quantum jumps” [Fig. 1(c)], providing strong evidence that the splitting does, indeed, originate from a single spin coupled to the electron. Occasionally, both sides of the split peak produces no resonance, indicating that the ^{31}P nuclear spin has flipped to $|\downarrow_{\text{P}}\rangle$. Therefore, we periodically measure the state of the donor nuclear spin and initialize it in the $|\uparrow_{\text{P}}\rangle$ state if it has flipped (see the Supplemental Material [23]).

To describe the NMR experiment on the single ^{29}Si nucleus, we adopt the following spin Hamiltonian [24,25]:

$$\mathcal{H} = -B_0(\gamma_e S_z + \gamma_{\text{P}} I_z^{\text{P}} + \gamma_{\text{Si}} I_z^{\text{Si}}) + A_{\text{P}} S \cdot I^{\text{P}} + A_{\text{Si}} S \cdot I^{\text{Si}}, \quad (1)$$

where S , I^{P} , and I^{Si} are the electron, ^{31}P , and ^{29}Si spin operators, and $\gamma_e = -28$ GHz/T, $\gamma_{\text{P}} = 17.23$ MHz/T, and $\gamma_{\text{Si}} = -8.458$ MHz/T (see Ref. [21]) are their respective gyromagnetic ratios. We assume that the electron- ^{29}Si interaction A_{Si} is dominated by a contact hyperfine term; i.e., we omit the dipolar coupling between ^{29}Si and the electron. This omission is justified by the fact that we observe an extremely small probability to flip the ^{29}Si spin through ionization and neutralization of the donor (~ 1 flip every 100 000 readout events), which indicates that the secular approximation for the electron-nuclear interaction is almost exact, and nondiagonal interaction terms are negligible. For this reason, the nuclear spin measurement is almost exactly quantum nondemolition (QND) [26].

Calling $\nu_{\text{Si}1}$ the ^{29}Si NMR frequency for a $|\uparrow\rangle$ electron, and $\nu_{\text{Si}2}$ for $|\downarrow\rangle$ [Fig. 2(b)], one has $\nu_{\text{Si}1,2} = |\gamma_{\text{Si}}| B_0 \mp |A_{\text{Si}}|/2$, since both γ_{Si} and A_{Si} are negative [21]. The ^{29}Si hyperfine splitting observed in Fig. 1(b) is ≈ 2.2 MHz at $B_0 = 1.77$ T, from which we estimate $\nu_{\text{Si}1} \approx 13.88$ MHz

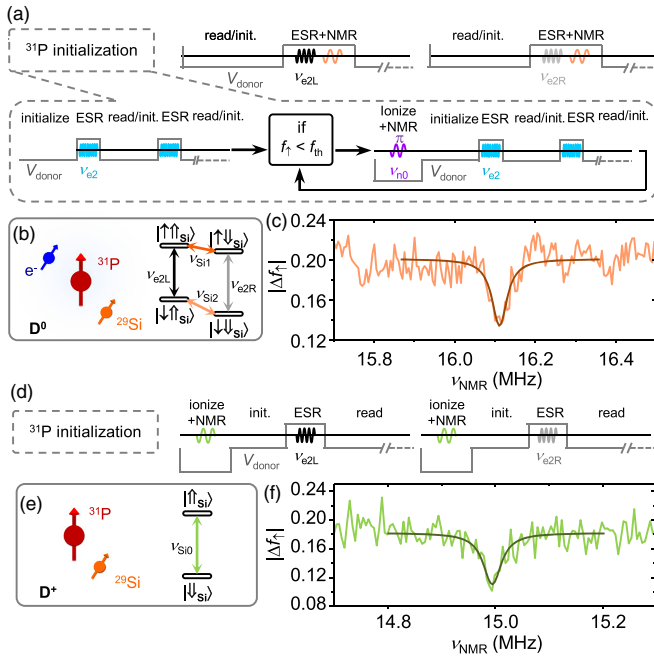


FIG. 2 (color online). (a) Pulse sequence, adapted from Ref. [3], for observing the ^{29}Si NMR frequencies. Here, V_{donor} represents a series of voltage pulses applied to an electrode above the donor to control the electrochemical potential of the bound electron. Preceding the NMR experiment is an initialization of the ^{31}P nuclear spin (see the Supplemental Material [23]). (b) Energy level diagram of the neutral (D^0) ^{29}Si : ^{31}P system, with corresponding ESR and NMR transitions, assuming a fixed ^{31}P nuclear spin state $|\uparrow_p\rangle$ ($m_p = +1/2$). (c) Absolute electron spin-up fraction difference $|\Delta f_\uparrow|$ as a function of the NMR frequency ν_{NMR} , for the ^{29}Si spin with a neutral donor and $m_e = -1/2$, $m_p = +1/2$. The resonance is best fit by a Lorentzian function, suggesting power broadening. (d) Pulse sequence, and (e) energy level diagram for ^{29}Si NMR transition at $\nu_{\text{Si}0}$ in the ionized donor (D^+). The $|\uparrow_{\text{Si}}\rangle$ state is highest in energy as a result of the negative value of the ^{29}Si nuclear gyromagnetic ratio. (f) NMR signal for the $\nu_{\text{Si}0}$ transition, with a Lorentzian fit.

and $\nu_{\text{Si}2} \approx 16.08$ MHz. Experimentally, the NMR frequencies are found by applying a long radio-frequency pulse at a frequency ν_{NMR} before or after a frequency-swept ESR pulse to adiabatically invert the electron [22], followed by the electron spin readout and reinitialization. The sequence is repeated for ESR frequencies centered around the two possible resonances $\nu_{e2L,R} = |\gamma_e|B_0 \mp |A_{\text{Si}}|/2$, dependent on the ^{29}Si spin state. We record the electron spin-up fractions $f_\uparrow(\nu_{e2L/R})$ at the two ESR frequencies, calculate the difference $|\Delta f_\uparrow| = |f_\uparrow(\nu_{e2R}) - f_\uparrow(\nu_{e2L})|$, and repeat the experiment at different values of ν_{NMR} .

In Fig. 2(c), we plot $|\Delta f_\uparrow(\nu_{\text{NMR}})|$ for the frequency interval around $\nu_{\text{Si}2}$. Off-resonance, we find $|\Delta f_\uparrow| \approx 0.21$. This value is reduced from the $|\Delta f_\uparrow|$ reported in Fig. 1(c) due to quantum jumps of the ^{31}P nuclear spin in between initialization stages and additional heating caused by the long NMR pulse. At resonance ($\nu_{\text{NMR}} \approx \nu_{\text{Si}2}$), the NMR

excitation randomizes the ^{29}Si spin state and tends to equalize the probability of having an “active” ν_{e2L} or ν_{e2R} ESR transition. The trough in $|\Delta f_\uparrow(\nu_{\text{NMR}})|$ is observed at $\nu_{\text{NMR}} = 16.11(2)$ MHz, remarkably close to the estimated value for $\nu_{\text{Si}2}$. Applying the NMR pulse before or after the ESR sweep should ideally determine whether the electron is initialized $|\downarrow\rangle$ or $|\uparrow\rangle$ while NMR is performed and, thus, determine whether a resonance is observed at $\nu_{\text{Si}2}$ or $\nu_{\text{Si}1}$. However, the thermal broadening of the SET island states causes a sizable probability of loading an $|\uparrow\rangle$ state at the start of the sequence. This is why the $\nu_{\text{Si}2}$ resonance is still observable (with a $\sim 30\%$ dip in $|\Delta f_\uparrow|$) even when an ESR pulse precedes the NMR pulse, as sketched in Fig. 2(a).

The tunnel-coupled SET used for readout can also be utilized to ionize the ^{31}P donor and perform NMR on the isolated ^{29}Si nuclear spin [Fig. 2(e)]. Here, the NMR frequency is simply $\nu_{\text{Si}0} = \gamma_{\text{Si}}B_0$. The pulse sequence for such a measurement is shown in Fig. 2(d) with the resulting resonance plot in Fig. 2(f). The trough at $\nu_{\text{NMR}} = 14.99(2)$ MHz, together with the external magnetic field $B_0 = 1.77$ T—calibrated using the measured ^{31}P NMR frequencies [3]—implies a gyromagnetic ratio of $|\gamma_{\text{Si}}| = 8.47$ MHz/T, very close to the bulk value of 8.458 MHz/T (see Ref. [21]). These experiments also yield an accurate value for the hyperfine coupling $|A_{\text{Si}}| = 2 \times (\nu_{\text{Si}2} - \nu_{\text{Si}0}) = 2.205(5)$ MHz.

We demonstrate the ability to coherently manipulate the ^{29}Si nuclear spin—with both a neutral (D^0) and ionized (D^+) donor—by observing Rabi oscillations. The ^{31}P nuclear spin is first initialized in the $|\uparrow_p\rangle$ state, followed by the loading of a $|\downarrow\rangle$ electron (or removal of the electron) and a NMR pulse at $\nu_{\text{Si}2}$ ($\nu_{\text{Si}0}$). A projective measurement of the ^{29}Si spin is then performed, leaving it initialized for the next cycle. The sequence is repeated 200 times for each pulse duration t_p and the ^{29}Si nuclear spin flip probability P_n is calculated. The ^{29}Si initialization fidelity is equivalent to the QND nuclear spin readout fidelity. The quantum jumps of the ^{29}Si nuclear spin [Fig. 1(c)] occur on a time scale of $T_{\text{flip}} \approx 10$ mins and represent a deviation from QND ideality. This time scale can be compared to the single-shot measurement time $T_{\text{meas}} \approx 104$ ms to give an estimate of the ^{29}Si initialization fidelity, i.e., $\exp(-T_{\text{meas}}/T_{\text{jump}}) > 99\%$. The protocols for the Rabi experiments are illustrated in Figs. 3(a) and 3(c), and the ^{29}Si nuclear spin flip probabilities as a function of the pulse duration are shown in Figs. 3(b) and 3(d) for the donor in the D^0 and D^+ charge states, respectively. The D^+ data display higher visibility oscillations than the D^0 case, due to its immunity to electron spin state initialization errors [2].

Next, we probe the coherence of the isolated (ionized donor) ^{29}Si nuclear spin by performing Ramsey fringe and Hahn echo experiments (Fig. 3). Fitting the Ramsey data in Fig. 3(e) with a damped cosine function of the form $P_n = P_n(0) \cos(2\pi\Delta d\tau) \exp(-\tau/T_2^*)$ yields a dephasing time of $T_2^* = 2.4(3)$ ms. Also, from this fit, we get Δd , the

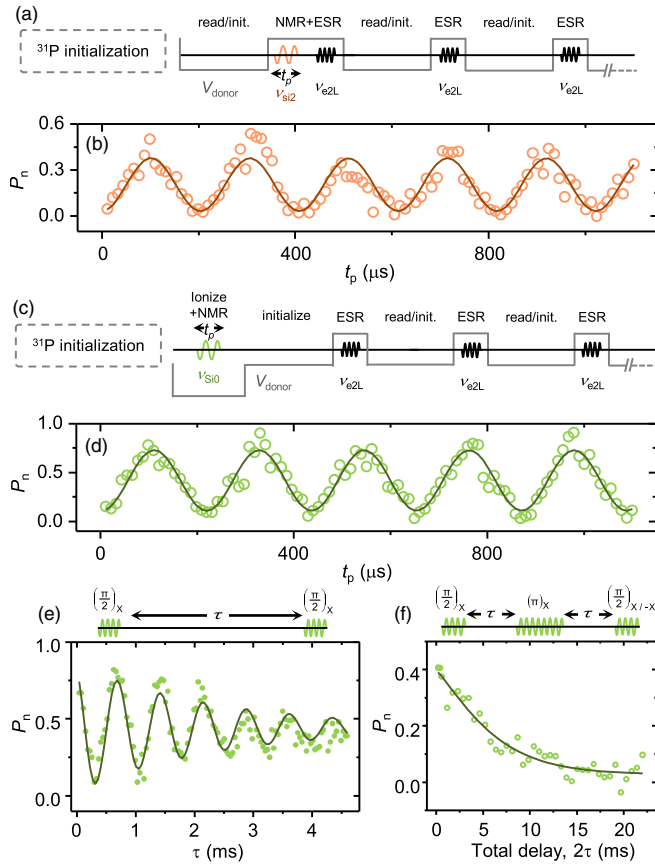


FIG. 3 (color online). (a) Protocol and (b) measurement of single ^{29}Si nuclear spin Rabi oscillations, i.e., nuclear spin flip probability P_n as a function of the pulse duration t_p , for the neutral donor with $m_e = -1/2$ and $m_p = +1/2$. (c) Protocol and (d) measurement of ^{29}Si Rabi oscillations with an ionized ^{31}P donor. Fits for both curves [(b) and (d)] are of the form $P_n \propto \sin^2(\pi f_{\text{Rabi}} t_p)$, where the Rabi frequency f_{Rabi} is a free fitting parameter. (e) Ramsey fringe measurement. (f) Hahn echo decay measured with phase cycling (between X and $-X$) of the final $\pi/2$ pulse in order to ensure a zero baseline. Fits to data in (e) and (f) are described in the main text.

average detuning from resonance, which enables us to provide a more accurate estimate of the gyromagnetic ratio $|\gamma_{\text{Si}}| = 8.460(2)$ MHz/T. The echo decay curve of Fig. 3(f), fitted with an exponential function $y = y(0) \exp((-2\tau/T_2)^b)$, reveals a coherence time $T_2 = 6.3(7)$ ms and an exponent $b = 1.2(2)$. The coherence time is in excellent agreement with Hahn echo measurements in bulk [27], where decoherence is caused by the dipole interactions with other ^{29}Si nuclear spins.

The individual hyperfine couplings between ^{29}Si nuclei and a donor-bound electron are known from early work in bulk samples [21,28–32]. By adapting metrology techniques demonstrated for ^{31}P [33], we can narrow down the possible locations of the ^{29}Si atom measured here. A device-specific electron wave function $\psi(r)$ was obtained by first calculating, with a finite-elements Poisson equation

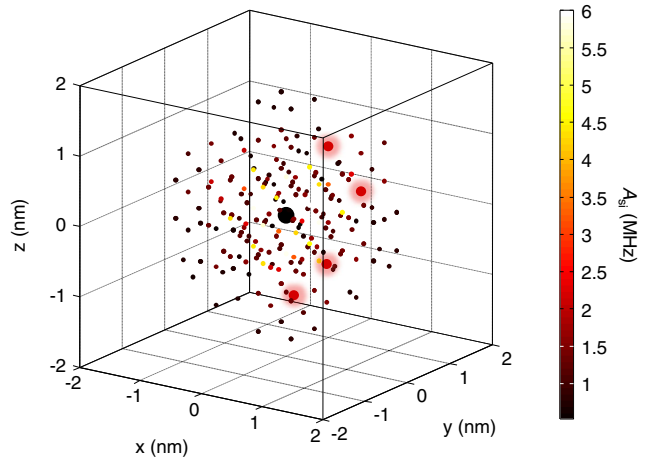


FIG. 4 (color online). Atomistic modeling to match the experimental hyperfine coupling. Plotted are the ^{29}Si nuclear spins with known hyperfine couplings [21]. The color scale indicates the hyperfine interaction at each site, rescaled to reflect the distorted donor electron wave function in our specific device. The lattice sites that correspond to couplings within the range 2.15–2.25 MHz are shown as larger circles.

solver, the electrostatic potential profile surrounding the donor, then solving the full atomistic tight-binding Hamiltonian with the nanoelectronic modeling tool NEMO 3D [34]. The strong electric fields (>3 MV/m [33]) in the nanostructure cause a distortion of the electron wave function, resulting in a Stark shift of $A_{\text{Si}} \propto |\psi(r_{\text{Si}})|^2$ from the bulk value. We calculated A_{Si} at several lattice sites near the ^{31}P nucleus (Fig. 4), and found four Si lattice sites where A_{Si} is in the range 2.15–2.25 MHz, shown as enlarged circles in Fig. 4. They all belong to a $(3, 3, \bar{7})$ shell at 1.11 nm distance from the ^{31}P nucleus (see the Supplemental Material [23]). We have, thus, been able to narrow down the location of our ^{29}Si atom to 4 out of a known ~ 204 possible sites. We found 34 lattice sites belonging to the shells $(0,0,4)$, $(4,4,0)$, $(3, 3, \bar{3})$, and $(3, 3, \bar{7})$ where $A_{\text{Si}} \geq 2$ MHz, which could potentially host a ^{29}Si qubit detectable with the methods described here.

In conclusion, we have performed an electrical single-shot QND readout on a single ^{29}Si nuclear spin, and demonstrated its coherent control through Rabi, Ramsey, and Hahn echo experiments, which yield coherence values similar to those observed in bulk samples. While the isotopic purification of ^{28}Si is an exciting avenue to achieve the best possible coherence and fidelity benchmarks [35], the present work shows that isolated ^{29}Si nuclear spins can be utilized as an additional resource [8] for quantum information processing in silicon.

We thank S. Vasiliev and W. A. Coish for discussions. This research was funded by the Australian Research Council Centre of Excellence for Quantum Computation and Communication Technology (Project No. CE110001027) and the U.S. Army Research Office

(Grant No. W911NF-13-1-0024). We acknowledge support from the Australian National Fabrication Facility. Computational resources on nanoHUB.org, funded by the NSF Grant No. EEC-0228390, were used in this work.

*Present address: London Centre for Nanotechnology, University College London, 17-19 Gordon Street, London WC1H 0AH, United Kingdom

j.pla@ucl.ac.uk

†a.morello@unsw.edu.au

- [1] J. R. Klauder and P. W. Anderson, *Phys. Rev.* **125**, 912 (1962).
- [2] J. J. Pla, K. Y. Tan, J. P. Dehollain, W. H. Lim, J. J. Morton, D. N. Jamieson, A. S. Dzurak, and A. Morello, *Nature (London)* **489**, 541 (2012).
- [3] J. J. Pla, K. Y. Tan, J. P. Dehollain, W. H. Lim, J. J. Morton, F. A. Zwanenburg, D. N. Jamieson, A. S. Dzurak, and A. Morello, *Nature (London)* **496**, 334 (2013).
- [4] R. Hanson, V. Dobrovitski, A. Feiguin, O. Gywat, and D. Awschalom, *Science* **320**, 352 (2008).
- [5] W. A. Coish and D. Loss, *Phys. Rev. B* **72**, 125337 (2005).
- [6] W. Yao, R.-B. Liu, and L. J. Sham, *Phys. Rev. B* **74**, 195301 (2006).
- [7] M. V. G. Dutt, L. Childress, L. Jiang, E. Togan, J. Maze, F. Jelezko, A. S. Zibrov, P. R. Hemmer, and M. D. Lukin, *Science* **316**, 1312 (2007).
- [8] L. Robledo, L. Childress, H. Bernien, B. Hensen, P. F. Alkemade, and R. Hanson, *Nature (London)* **477**, 574 (2011).
- [9] G. Waldherr *et al.*, *Nature (London)* **506**, 204 (2014).
- [10] T. H. Taminiau, J. Cramer, T. van der Sar, V. V. Dobrovitski, and R. Hanson, *Nat. Nanotechnol.* **9**, 171 (2014).
- [11] N. H. Nickerson, Y. Li, and S. C. Benjamin, *Nat. Commun.* **4**, 1756 (2013).
- [12] T. D. Ladd, J. R. Goldman, F. Yamaguchi, Y. Yamamoto, E. Abe, and K. M. Itoh, *Phys. Rev. Lett.* **89**, 017901 (2002).
- [13] K. M. Itoh, *Solid State Commun.* **133**, 747 (2005).
- [14] A. Morello, C. C. Escott, H. Huebl, L. H. Willems van Beveren, L. C. L. Hollenberg, D. N. Jamieson, A. S. Dzurak, and R. G. Clark, *Phys. Rev. B* **80**, 081307 (2009).
- [15] D. N. Jamieson, C. Yang, T. Hopf, S. M. Hearne, C. I. Pakes, S. Prawer, M. Mitic, E. Gauja, S. E. Andresen, F. E. Hudson, A. S. Dzurak, and R. G. Clark, *Appl. Phys. Lett.* **86**, 202101 (2005).
- [16] S. J. Angus, A. J. Ferguson, A. S. Dzurak, and R. G. Clark, *Nano Lett.* **7**, 2051 (2007).
- [17] A. Morello *et al.*, *Nature (London)* **467**, 687 (2010).
- [18] J. P. Dehollain, J. J. Pla, E. Siew, K. Y. Tan, A. S. Dzurak, and A. Morello, *Nanotechnology* **24**, 015202 (2013).
- [19] A. M. Tyryshkin, S. A. Lyon, A. V. Astashkin, and A. M. Raitsimring, *Phys. Rev. B* **68**, 193207 (2003).
- [20] J. Järvinen *et al.*, *Phys. Rev. B* **90**, 214401 (2014).
- [21] E. B. Hale and R. L. Mieher, *Phys. Rev.* **184**, 739 (1969).
- [22] A. Laucht, R. Kalra, J. T. Muhonen, J. P. Dehollain, F. A. Mohiyaddin, F. Hudson, J. C. McCallum, D. N. Jamieson, A. S. Dzurak, and A. Morello, *Appl. Phys. Lett.* **104**, 092115 (2014).
- [23] See Supplemental Material at <http://link.aps.org/supplemental/10.1103/PhysRevLett.113.246801> for extended figure captions.
- [24] G. Feher, *Phys. Rev.* **114**, 1219 (1959).
- [25] M. H. Levitt, *Spin Dynamics: Basics of Nuclear Magnetic Resonance* (Wiley, New York, 2008).
- [26] V. B. Braginsky and F. Y. Khalili, *Rev. Mod. Phys.* **68**, 1 (1996).
- [27] A. E. Dementyev, D. Li, K. MacLean, and S. E. Barrett, *Phys. Rev. B* **68**, 153302 (2003).
- [28] E. B. Hale and R. L. Mieher, *Phys. Rev.* **184**, 751 (1969).
- [29] E. B. Hale and R. L. Mieher, *Phys. Rev. B* **3**, 1955 (1971).
- [30] J. L. Ivey and R. L. Mieher, *Phys. Rev. Lett.* **29**, 176 (1972).
- [31] J. L. Ivey and R. L. Mieher, *Phys. Rev. B* **11**, 822 (1975).
- [32] J. L. Ivey and R. L. Mieher, *Phys. Rev. B* **11**, 849 (1975).
- [33] F. A. Mohiyaddin, R. Rahman, R. Kalra, G. Klimeck, L. C. L. Hollenberg, J. J. Pla, A. S. Dzurak, and A. Morello, *Nano Lett.* **13**, 1903 (2013).
- [34] G. Klimeck, S. Ahmed, H. Bae, N. Khariche, S. Clark, B. Haley, S. Lee, M. Naumov, H. Ryu, F. Saied, M. Prada, M. Korkusinski, T. Boykin, and R. Rahman, *IEEE Trans. Electron Devices* **54**, 2079 (2007).
- [35] J. T. Muhonen, J. P. Dehollain, A. Laucht, F. E. Hudson, T. Sekiguchi, K. M. Itoh, D. N. Jamieson, J. C. McCallum, A. S. Dzurak, and A. Morello *Nat. Nanotechnol.* **9**, 986 (2014).